We have demonstrated through structure-guided design that neutralization of positive charges in the nt-groove can dramatically decrease off-target indel formation while preserving on-target activity. These data show that eSpCas9(1.1) can be used to increase the specificity of genome-editing applications. Future structure-guided interrogation of Cas9 binding and cleavage mechanism will likely enable further optimization of the CRISPR-Cas9 genome-editing toolbox.

REFERENCES AND NOTES

1. L. Cong *et al.*, *Science* **339**, 819–823 (2013).
2. P. Mali *et al.*, *Science* **339**, 823–826 (2013).
3. P. D. Hsu *et al.*, *Nat. Biotechnol.* **31**, 827–832 (2013).
4. Y. Fu *et al.*, *Nat. Biotechnol.* **31**, 822–826 (2013).
5. B. Zetsche, S. E. Volz, F. Zhang, *Nat. Biotechnol.* **33**, 139–142 (2015).
6. K. M. Davis, V. Pattanayak, D. B. Thompson, J. A. Zuris, D. R. Liu, *Nat. Chem. Biol.* **11**, 316–318 (2015).
7. F. A. Ran *et al.*, *Cell* **154**, 1380–1389 (2013).
8. P. Mali *et al.*, *Nat. Biotechnol.* **31**, 833–838 (2013).
9. Y. Fu, J. D. Sander, D. Reyon, V. M. Cascio, J. K. Joung, *Nat. Biotechnol.* **32**, 279–284 (2014).
10. S. Q. Tsai *et al.*, *Nat. Biotechnol.* **32**, 569–576 (2014).
11. J. P. Guilinger, D. B. Thompson, D. R. Liu, *Nat. Biotechnol.* **32**, 577–582 (2014).
12. Y. Fu, J. D. Sander, D. Reyon, V. M. Cascio, J. K. Joung, *Nat. Biotechnol.* **32**, 279–284 (2014).
13. S. Q. Tsai *et al.*, *Nat. Biotechnol.* **33**, 187–197 (2015).
14. H. Nishimasu *et al.*, *Cell* **156**, 935–949 (2014).
15. C. Anders, O. Niewoehner, A. Duerst, M. Jinek, *Nature* **513**, 569–573 (2014).
16. E. Semenova *et al.*, *Proc. Natl. Acad. Sci. U.S.A.* **108**, 10098–10103 (2011).
17. B. Wiedenheft *et al.*, *Proc. Natl. Acad. Sci. U.S.A.* **108**, 10092–10097 (2011).
18. W. Jiang, D. Bikard, D. Cox, F. Zhang, L. A. Marraffini, *Nat. Biotechnol.* **31**, 233–239 (2013).
19. S. H. Sternberg, S. Redding, M. Jinek, E. C. Greene, J. A. Doudna, *Nature* **507**, 62–67 (2014).
20. N. Crosetto *et al.*, *Nat. Methods* **10**, 361–365 (2013).
21. F. A. Ran *et al.*, *Nature* **520**, 186–191 (2015).

ACKNOWLEDGMENTS

We thank J. Dahlman for helpful discussions and a critical review of the manuscript; F. A. Ran, R. J. Platt, and J. Joung for experimental assistance; and the entire Zhang laboratory for support and advice. I.S. is supported by the Simons Center for the Social Brain. W.X.Y. is supported by T32GM007753 from the National Institute of General Medical Sciences and a Paul and Daisy Soros Fellowship. F.Z. is supported by the National Institutes of Health through NIMH (5DP1-MH100706 and 1R01MH110049) and NIDDK (5R01DK097768-03), a Waterman Award from the National Science Foundation, the Keck, New York Stem Cell, Damon Runyon, Searle Scholars, Merkin, and Vallee Foundations, and B. Metcalfe. F.Z. is a New York Stem Cell Foundation Robertson Investigator. I.S., L.G., B.Z., and F.Z. are inventors on provisional patent application 62/181,453 applied for by the Broad Institute and MIT that covers the engineered CRISPR proteins described in this manuscript. Plasmid DNA encoding eSpCas9(1.0) and eSpCas9(1.1) are available from Addgene under a Universal Biological Material Transfer Agreement with the Broad Institute and MIT. F.Z. is a founder and scientific advisor for Editas Medicine and a scientific advisor for Horizon Discovery. Further information about the protocols, plasmids, and reagents can be found at the Zhang laboratory website (www.genome-engineering.org).

SUPPLEMENTARY MATERIALS

www.sciencemag.org/content/351/6268/84/suppl/DC1
Materials and Methods
Figs. S1 to S12
Tables S1 to S3
Supplementary DNA Sequences
References

24 September 2015; accepted 18 November 2015
Published online 1 December 2015
10.1126/science.aad5227

PROTEIN TRANSLOCATION

Structure of the Sec61 channel opened by a signal sequence

Rebecca M. Voorhees and Ramanujan S. Hegde*

Secreted and integral membrane proteins compose up to one-third of the biological proteome. These proteins contain hydrophobic signals that direct their translocation across or insertion into the lipid bilayer by the Sec61 protein–conducting channel. The molecular basis of how hydrophobic signals within a nascent polypeptide trigger channel opening is not understood. Here, we used cryo–electron microscopy to determine the structure of an active Sec61 channel that has been opened by a signal sequence. The signal supplants helix 2 of Sec61α, which triggers a rotation that opens the central pore both axially across the membrane and laterally toward the lipid bilayer. Comparisons with structures of Sec61 in other states suggest a pathway for how hydrophobic signals engage the channel to gain access to the lipid bilayer.

The universally conserved Sec complex forms a gated protein translocation channel at the eukaryotic endoplasmic reticulum (ER) and bacterial plasma membrane (*1*). The central component of this channel, SecY in bacteria and Sec61α in eukaryotes, contains 10 transmembrane (TM) helices arranged around a central pore (*2*). Two single-TM subunits in eukaryotes, Sec61β and Sec61γ, are peripheral to Sec61α. The central pore in the inactive Sec complex is occluded by a short "plug" helix that must be displaced to allow translocation. The interface where TM helices 2 and 3 contact helices 7 and 8 defines a "lateral gate" for membrane access of polypeptides (*1–3*).

Crystal structures of the Sec complex (*2*, *4–6*) lack a translocating polypeptide and likely represent a range of inactive states. Depending on crystal contacts or translocation partners, the lateral gate and plug are in various states of opening and displacement. However, the biological relevance of these channel conformations has been difficult to interpret without a well-resolved and matched active structure. Previous structures of translocation or insertion intermediates of the ribosome-Sec complex determined by cryo–electron microscopy (cryo-EM) were of moderate resolution (*7–9*), contained heterogeneous substrates (*9*), required artificial stabilization (*8*), or were at an uncertain stage of insertion (*7*). Although these earlier structures provided the first views of substrate-induced structural changes consistent with lateral gate opening, the data could not clearly resolve individual Sec61 TM helices or the nature of their interactions with the signal. Thus, a molecular understanding of how substrates open the channel for translocation or insertion is incomplete.

We devised a strategy to tag and purify the canine ribosome-Sec61 complex engaged by the first 86 residues of the secretory protein preprolactin (fig. S1). Translocation, protease-protection, and photo–cross-linking experiments verified that, like the well-characterized native 86-residue intermediate (*10–15*), our tagged complex represents a functional translocation intermediate engaged by Sec61 (figs. S2 to S4). The nascent polypeptide remains engaged with Sec61 during and after purification (fig. S4), which makes it suitable for structure determination by single-particle cryo-EM.

The structure of this engaged ribosome-Sec61 complex was reconstructed from 101,339 particles to an overall resolution of 3.6 Å (figs. S5 and S6 and table S1). The local resolution of the Sec61 channel ranged from ~ 3.5 Å near the ribosome to ~7.0 Å at the lumenal loops. Most TM helices were at ~4.5 to 5.5 Å resolution (fig. S6), which revealed clear helical pitch and many bulky side chains in sharpened maps (fig. S7). All 12 TM helices of the Sec61 complex could be unambiguously assigned, leaving a single helix we ascribed to the signal sequence (Fig. 1, A and B, and fig. S8). Density visible throughout the ribosomal exit tunnel and in parts of the Sec61 channel (Fig. 1C) suggests a looped configuration for the nascent chain, consistent with earlier cross-linking studies (*11*).

The well-resolved structure of a biochemically validated early translocation intermediate permitted detailed comparisons with other Sec61 states to gain insights into the conformational changes accompanying channel opening. A previous cryo-EM structure of the porcine ribosome-Sec61 complex lacking a nascent polypeptide (*9*) represents a "primed" state preceding nascent chain insertion. Relative to this primed structure, the engaged channel is open laterally toward the lipid bilayer and axially across the membrane (Fig. 2). The ribosome-Sec61 interaction remains fixed, with only minor movements of the associated Sec61γ and TM helices 6, 7, 8, and 9 of Sec61α. The other seven TM helices of the Sec61 complex rotate as a rigid body by ~22° (Fig. 2A and movies S1 and S2), which creates space between helices 2 and 7 for intercalation of the signal peptide (Fig. 2B). Notably, cryo-tomography

MRC Laboratory of Molecular Biology, Medical Research Council, Francis Crick Avenue, Cambridge CB2 0QH, UK.
***Corresponding author. E-mail: rhegde@mrc-lmb.cam.ac.uk**

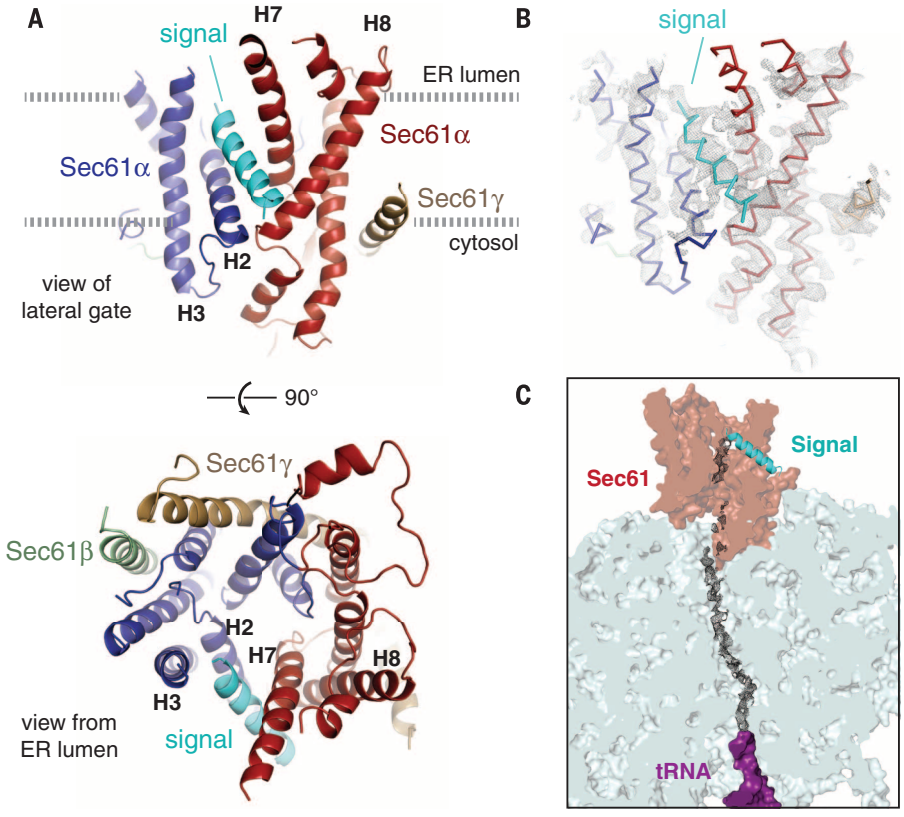

Fig. 1. Structure of the signal peptide-engaged Sec61 complex. (**A**) View of the lateral gate (top) or from the ER lumen of the Sec61 complex bound to the preprolactin signal peptide (cyan). The mobile regions of Sec61α are blue; the comparatively immobile regions are red. The β and γ subunits are pale green and tan, respectively. Helices that compose the lateral gate are labeled. (**B**) Experimental density for the structure (mesh, filtered to 4.5 Å resolution) superimposed on the backbone trace of the structural model. (**C**) Density observed for the nascent polypeptide through the ribosomal tunnel and parts of the Sec61 channel.

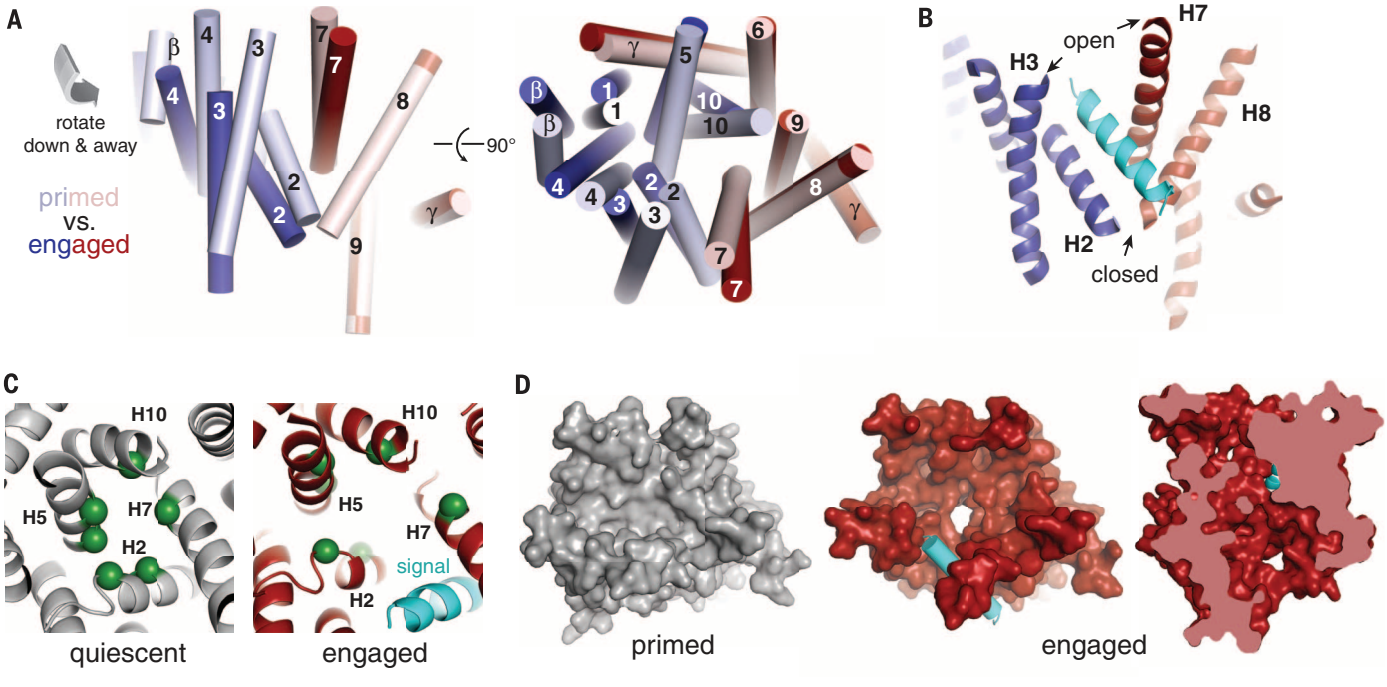

Fig. 2. Conformational changes to Sec61 upon engagement by a signal peptide. (**A**) Positions of the transmembrane helices of the Sec61 complex in the ribosome-primed (pale colors, PDB 3J7Q) and signal-engaged (bright colors) states. The mobile regions of Sec61α are blue; the comparatively immobile regions are red. Individual helices are labeled; the signal has been omitted for clarity. (**B**) View of the asymmetrically opened lateral gate. (**C**) View of the pore ring residue positions (green spheres) in the quiescent SecY crystal structure (gray, PDB 1RH5) and engaged Sec61 complex (red). The signal is cyan. (**D**) (Left and middle) Surface view of the primed (gray, PDB 3J7Q) and engaged (red) states of the Sec61 complex viewed from the ER lumen. The lumenal loops have been removed for clarity. The signal peptide is cyan. (Right) cutaway view perpendicular to the membrane of the engaged Sec61 complex showing an open channel.

of the Sec61 complex in native ER microsomes shows a similar configuration (*16*). Although the heterogeneous and uncertain functional state of the cryo-tomography structure complicates its placement within the translocation cycle (*17*), it does illustrate that our engaged structure is likely to be compatible with a membrane environment.

Because the 22° rotation is oblique relative to the plane of the membrane, lateral gate opening is asymmetric: the lumenal end of the gate parts by ~15 Å, whereas the cytosolic side remains closed (Fig. 2B). Oblique rotation of helices 2, 5, and 10 away from helix 7 displaces a set of six conserved "pore ring" residues (table S2) from their normally planar configuration (Fig. 2C). The plug is apparently destabilized by separation of the pore ring, atop which it ordinarily sits (*2*), which leads to an unobstructed conduit across the membrane (Fig. 2D). Thus, opening of the Sec61 channel is directly coupled to successful signal sequence recognition via its intercalation in the lateral gate.

To understand how the signal sequence reaches this position, we asked whether Sec61 priming by the ribosome might favor subsequent signal sequence engagement. For comparison, we used the *M. jannaschii* x-ray structure of an isolated Sec complex in its "quiescent" state (*2*), whose overall architecture, TM helix interactions, and key functional motifs (table S2) are well conserved in mammals. Relative to the quiescent channel, the ribosome-primed Sec61 complex is partially destabilized in two ways. First, a "polar cluster" of three residues on helices 2 and 7 that form stabilizing hydrogen bonds is separated in the primed state (Fig. 3A). Hence, the lateral gate is partially cracked in the precise region eventually occupied by the signal peptide. Second, the external surface of the primed Sec61 complex (Fig. 3B) contains a hydrophilic seam that is energetically disfavored by its exposure to the hydrophobic interior of the lipid bilayer. A similar conformational change is seen in the bacterial SecY complex bound to SecA (*6*). Thus, two diverse translocation partners from different translocation pathways, the ribosome and SecA, induce similar priming events by binding to the cytosolic loops of the Sec61 and SecY complex, respectively.

When viewed from the ribosomal exit tunnel, nearly all of the surfaces on the primed Sec61 complex available to a nascent signal peptide are hydrophilic. The only substantive hydrophobic patch, deep within the channel pore, might serve as the initial interaction site for a hydrophobic signal (Fig. 4A). This hydrophobic patch is composed of residues from the lateral gate and pore ring (table S2) and is positioned adjacent to the region of the lateral gate weakened by ribosome priming (Fig. 4B). Packing of the hydrophobic signal at this destabilized region may facilitate its intercalation into the lateral gate, driven by the energetically favorable exposure of the signal to lipid, so that it eventually adopts the conformation seen in our structure.

The position of the engaged signal perfectly supplants helix 2 and replaces its interactions with helices 7 and 8 to stabilize the open channel conformation (Fig. 4, C and D). Hydrophilic segments of polypeptide would not be energetically favored in this position, which explains why they cannot open the channel. The conserved hydrophobicity and length of helix 2 suggests that the biophysical properties of helix 2 may dictate what constitutes a functional signal for translocation, a property that is similar, but not identical across species. The concept of a hydrophobicity threshold set by an intramolecular "placeholder" is also used by the signal recognition particle at an earlier step of this pathway (*18*) and may be a general mechanism for increasing recognition fidelity of widely divergent sequences.

Our structure of the signal-engaged Sec61 translocon, together with earlier quiescent and primed structural states, leads to a molecular model for selective gating of the translocon by hydrophobic signals. Ribosome binding constrains the cytosolic loops of Sec61 to enforce a conformation in which key lateral gate contacts, including the conserved polar cluster, are weakened. A hydrophobic patch close to this site attracts hydrophobic signals to their point of initial engagement. If the signal is sufficiently hydrophobic, it can proceed further to displace the comparably hydrophobic helix 2 and access the lipid bilayer while simultaneously widening the central pore to destabilize the plug. Thus, polypeptides initially sample the cytosolic vestibule of Sec61 and gain access to the lipid bilayer via the channel interior, contingent on both a suitably hydrophobic signal and an appropriately primed translocation channel.

This stepwise model for translocon opening is consistent with fluorescence and cross-linking studies showing that signals are initially in an aqueous environment (*19*) near Sec61α (*10*–*13*) and only access lipid after further elongation (*13*, *15*). Furthermore, mutants of the lateral gate, plug, and pore ring residues in the hydrophobic patch

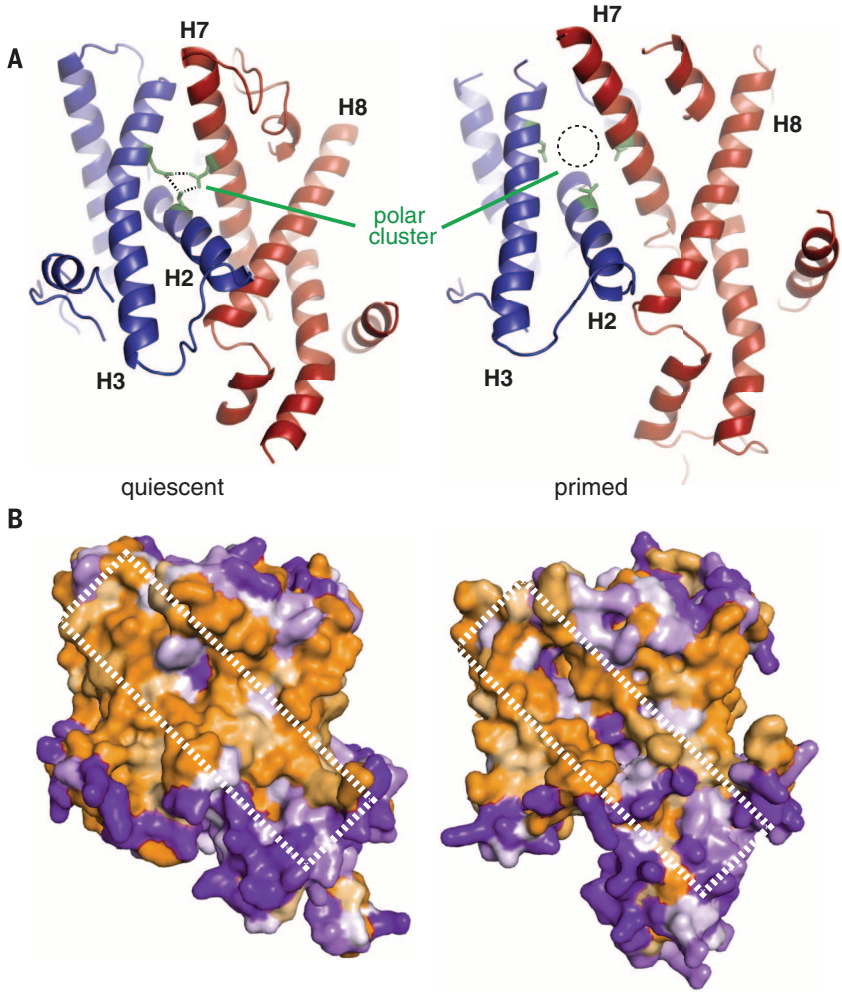

Fig. 3. The lateral gate is destabilized in the ribosome-primed Sec61 complex. (**A**) Comparison of the quiescent SecY (left, PDB 1RH5) and primed Sec61 (right, PDB 3J7Q) complexes. Ribosome binding results in partial destabilization of the lateral gate by shifting helices 2 and 3 away from the midline, which disrupts the polar cluster (green). (**B**) Space-filling model viewing the lateral gate of the quiescent (left) and primed (right) structures colored by hydrophobicity, in which orange is hydrophobic and purple is hydrophilic. The hydrophilic seam produced by ribosome binding is indicated.

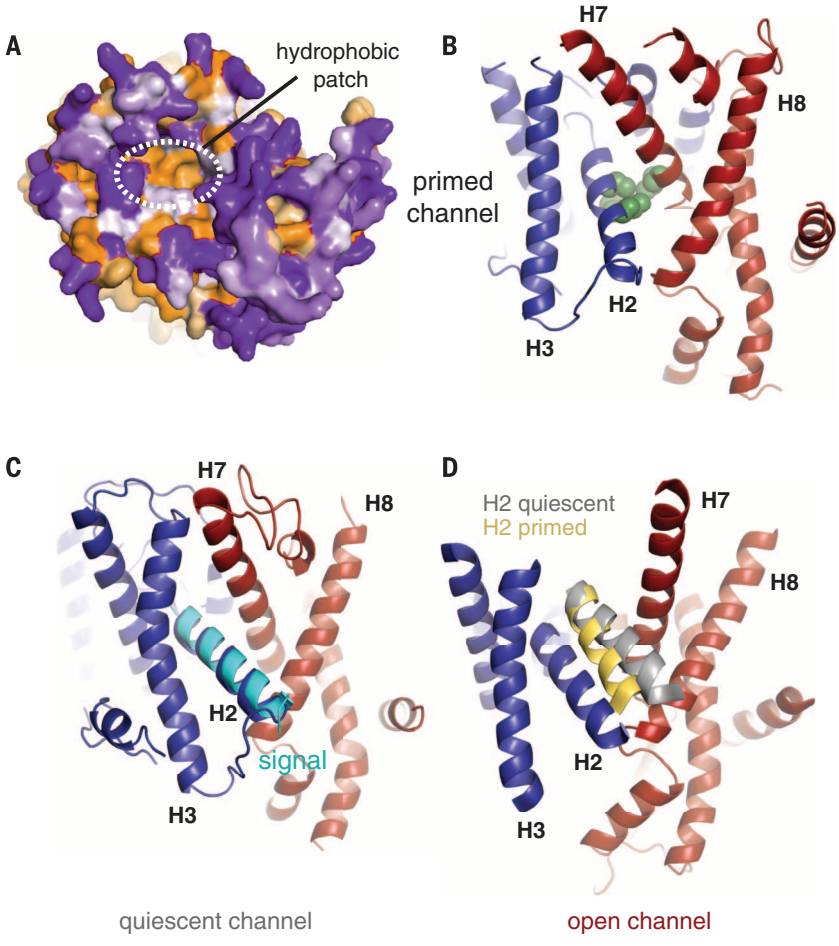

Fig. 4. Putative path of the signal peptide into the Sec61 lateral gate. (**A**) Space-filling model of the cytosolic vestibule of Sec61 viewed from the ribosome, colored by hydrophobicity as in Fig. 3B. (**B**) Residues comprising the hydrophobic patch are at the lateral gate. (**C**) The eventual position of the signal peptide (cyan), relative to the stationary ribosome-bound regions of Sec61, is essentially identical to the position of helix 2 in the quiescent state. (**D**) Positions of helix 2 in the quiescent (gray) and primed (yellow) states superimposed on the engaged Sec61 structure (red and blue). The signal peptide is omitted for clarity but would reside precisely in the position of the quiescent helix 2.

or polar cluster region allow crippled signal sequences to mediate translocation (*20*–*25*). It is possible that such mutants lead to a more dynamic Sec61 channel that can open without signal sequence intercalation into the lateral gate. This would bypass the signal recognition step captured by our structure and permit promiscuous translocation. Conversely, stabilization of lateral gate contacts increases the hydrophobic threshold for signal sequence–mediated translocation (*24*, *25*). Similarly, inhibitors that impede Sec61 opening are thought to bind at the plug and lateral gate junction (*26*, *27*). Thus, defining the location of a signal in the process of initiating translocation permits molecular interpretations of earlier functional data and provides a basis for future studies of other stages in protein translocation. Analysis of signals and TM domains of different biophysical properties in both defined and native translocon complexes will be crucial for understanding how the Sec61 translocon is able to handle the remarkably diverse substrates transiting the membrane.

REFERENCES AND NOTES

1. E. Park, T. A. Rapoport, *Annu. Rev. Biophys.* **41**, 21–40 (2012).
2. B. Van den Berg *et al.*, *Nature* **427**, 36–44 (2004).
3. K. Plath, W. Mothes, B. M. Wilkinson, C. J. Stirling, T. A. Rapoport, *Cell* **94**, 795–807 (1998).
4. P. F. Egea, R. M. Stroud, *Proc. Natl. Acad. Sci. U.S.A.* **107**, 17182–17187 (2010).
5. T. Tsukazaki *et al.*, *Nature* **455**, 988–991 (2008).
6. J. Zimmer, Y. Nam, T. A. Rapoport, *Nature* **455**, 936–943 (2008).
7. M. Gogala *et al.*, *Nature* **506**, 107–110 (2014).
8. E. Park *et al.*, *Nature* **506**, 102–106 (2014).
9. R. M. Voorhees, I. S. Fernández, S. H. W. Scheres, R. S. Hegde, *Cell* **157**, 1632–1643 (2014).
10. S. High *et al.*, *J. Biol. Chem.* **268**, 26745–26751 (1993).
11. W. Mothes, S. Prehn, T. A. Rapoport, *EMBO J.* **13**, 3973–3982 (1994).
12. B. Jungnickel, T. A. Rapoport, *Cell* **82**, 261–270 (1995).
13. W. Mothes, B. Jungnickel, J. Brunner, T. A. Rapoport, *J. Cell Biol.* **142**, 355–364 (1998).
14. K. S. Crowley, S. Liao, V. E. Worrell, G. D. Reinhart, A. E. Johnson, *Cell* **78**, 461–471 (1994).
15. B. Martoglio, M. W. Hofmann, J. Brunner, B. Dobberstein, *Cell* **81**, 207–214 (1995).
16. S. Pfeffer *et al.*, *Nat. Commun.* **6**, 8403 (2015).
17. Although P-site transfer RNA was absent from the majority of ribosomes used for the cryo-tomography structure (*16*), the presence or absence of heterogeneous endogenous nascent polypeptides within Sec61 could not be determined conclusively. Thus, the conclusion that the Sec61 complex is constitutively open upon ribosome binding, independent of substrate or functional state, may be premature. Indeed, biochemical studies in native microsomes show substrate-induced Sec61 opening (*14*), no translocation of Sec61-docked polypeptides with a mutant signal (*12*), and no lipid access to early translocation intermediates (*13*). Genetic studies show that modulation of lateral gate interactions influences translocation (*20*–*27*). Thus, multiple independent findings argue that substrates induce structural changes to the Sec61 complex that open it laterally.
18. R. M. Voorhees, R. S. Hegde, *eLife* **4**, e07975 (2015).
19. K. S. Crowley, G. D. Reinhart, A. E. Johnson, *Cell* **73**, 1101–1115 (1993).
20. T. Junne, T. Schwede, V. Goder, M. Spiess, *J. Biol. Chem.* **282**, 33201–33209 (2007).
21. M. A. Smith, W. M. J. Clemons Jr., C. J. DeMars, A. M. Flower, *J. Bacteriol.* **187**, 6454–6465 (2005).
22. A. I. Derman, J. W. Puziss, P. J. J. Bassford Jr., J. Beckwith, *EMBO J.* **12**, 879–888 (1993).
23. R. S. Osborne, T. J. Silhavy, *EMBO J.* **12**, 3391–3398 (1993).
24. A. P. Maillard, S. Lalani, F. Silva, D. Belin, F. Duong, *J. Biol. Chem.* **282**, 1281–1287 (2007).
25. S. F. Trueman, E. C. Mandon, R. Gilmore, *J. Cell Biol.* **199**, 907–918 (2012).
26. A. L. Mackinnon, V. O. Paavilainen, A. Sharma, R. S. Hegde, J. Taunton, *eLife* **3**, e01483 (2014).
27. T. Junne *et al.*, *J. Cell Sci.* **128**, 1217–1229 (2015).

ACKNOWLEDGMENTS

We thank F. de Haas, V. Ragunath, and C. Savva for help with data collection; S. Chen, G. McMullan, J. Grimmett, and T. Darling for technical support; S. Shao for helpful discussions. This work was supported by the UK Medical Research Council (MC_UP_A022_1007 to RSH) and a Wellcome Trust postdoctoral fellowship (R.M.V.). The Cryo-EM map for the engaged ribosome-Sec61 complex has been deposited with the EMDataBank (EMDB-3245). The Protein Data Bank accession number for the engaged Sec61 complex is 3JC2.

SUPPLEMENTARY MATERIALS

www.sciencemag.org/content/351/6268/88/suppl/DC1
Materials and Methods
Figs. S1 to S8
Tables S1 and S2
Captions for Movies S1 and S2
References (*28*–*46*)
Movies S1 and S2

21 September 2015; accepted 20 November 2015
10.1126/science.aad4992

Supplementary Materials for

Structure of the Sec61 channel opened by a signal sequence

Rebecca M. Voorhees and Ramanujan S. Hegde*

*Corresponding author. E-mail: rhegde@mrc-lmb.cam.ac.uk

Published 1 January 2016, *Science* **351**, 88 (2016)
DOI: 10.1126/science.aad4992

This PDF file includes

Other Supplementary Material for this manuscript includes the following:
(available at www.sciencemag.org/content/351/6268/88/suppl/DC1)

Materials and Methods

Plasmids, antibodies, and recombinant protein

An SP64 vector-based construct encoding bovine pre-prolactin (pPL) was modified to contain an N-terminal affinity tag (3xFLAG) and short glycine-serine linker to generate FLAG-pPL. The encoded protein sequence is shown in Fig. S1. The mammalian expression construct for GTPase-deficient Hbs1 (Hbs1-DN) has been described [*28*], and was purified as before [*29*]. Antibodies against uL6 (Santa Cruz, anti-L9) and uS9 (Santa Cruz, anti-S16) were purchased, and the antibodies against TRAPα, Sec61α, Sec61β and TRAM were characterized previously [*30, 11-13*]. Anti-Flag affinity resin and 3X Flag peptide were obtained from Sigma.

In vitro transcription, translation, and biochemical characterization

Preparation and purification of stalled ribosome nascent chain (RNC) complexes were performed using minor variations of previously described methods [*18,28-31*]. All in vitro translation reactions used the rabbit reticulocyte lysate system assembled as described before [*31*]. Canine pancreas derived rough microsomes (RMs) were prepared as described [32]. Analytic translation reactions for biochemical characterization were carried out using ^{35}S-methionine to detect the translated products, while preparative scale reactions for cryo-EM (described below) used unlabelled methionine. The template for in vitro transcription of the truncated RNC was prepared by PCR from the FLAG-pPL (or untagged pPL) constructs using a 5' primer preceding the SP6 promoter, and a 3' primer at codon 85 of native pPL. The 3' primer encoded a terminal valine as the 86th amino acid, whose peptidyl-tRNA is relatively resistant to spontaneous hydrolysis. Template for full length products used a 3' primer beyond the native stop codon. PCR products were purified and used for *in vitro* transcription as described [*31*].

Analytical translation reactions to characterize the FLAG-pPL construct (fig. S2-S4) were typically for 20-30 min at 32°C, with further manipulations and analysis performed on ice unless otherwise indicated. Protease protection of full length products (fig. S2A) used 0.5 mg/ml proteinase K at 0°C as described before [*30*]. Puromycin treatment (fig. S2B) used 1 mM puromycin for 15 min at 32°C. For photo-cross-linker incorporation, the charged suppressor tRNAs were obtained from tRNA Probes (catalog numbers A12 and A13). They were added to the translation reactions at a final concentration of ~1 μM. For cross-linking, the microsomes were sedimented from the total translation reactions by layering the sample on 100 μl of 25% sucrose (w/v) in 120 mM KOAc, 50 mM Hepes, pH 7.5, 2 mM $MgCl_2$ and centrifuging for 30 min at 55,000 rpm in a TLA55 rotor. After resuspension in the same buffer without sucrose, the samples were irradiated for 15 min on ice ~10 cm from the light source of a UVP B-100 series lamp (UVP LLC). Immunoprecipitations for Sec61α and TRAM cross-linked products were as before [*33*]. The protease-protection assay for insertion into the Sec61 channel (fig. S4) was performed as described previously [*12, 13*]. Where indicated, deacylation of the tRNA prior to SDS-PAGE was performed by adjusting the sample to pH ~12, incubation for 15 min at 37°C, and neutralization with sample buffer.

Sample preparation for EM analysis

Preparative scale RNC purification for EM analysis utilized rabbit reticulocyte lysate that was first depleted of 80S ribosomes by centrifugation for 75 min at 50,000 rpm in a Beckman TLA55 rotor. The resulting supernatant was used in a 3.5-ml translation reaction containing canine pancreatic rough microsomes at a final A_{280} of ~12. Translation occurs on membrane-bound ribosomes contributed from the microsomes, maximizing translocon engagement. After incubation for 5 min at 32° C to initiate translation, Hbs1-DN was added to ~133 nM, and incubated for a further 20 min at 32° C. Note that the Hbs1-DN inhibits ribosome splitting and engagement of the ribosome-associated quality control pathway [31], thereby ensuring a more homogeneous RNC population. The resulting membranes were then pelleted by centrifugation for 20 min at 50,000 rpm in a TLA55 rotor, and resuspended in membrane buffer (50 mM HEPES pH 7.5, 250 mM sucrose, 2 mM $MgOAc_2$) to one-tenth the volume of the initial translation reaction. Solubilization was carried out by addition of an equal volume of 2x solubilisation buffer (3.5% digitonin, 100 mM HEPES pH 7.5, 800 mM KOAc, 20 mM $MgOAc_2$, 2 mM DTT) and incubated 10 minutes on ice. Samples were centrifuged for 15 min at 20,000 x g at 4° C to remove insoluble material, and then diluted 10-fold in column buffer (50 mM HEPES pH 7.5, 200 mM KOAc, 15 mM $MgOAc_2$, 1 mM DTT). Note that the digitonin used throughout the solubilization and purification was purified further from the commercially obtained preparation (from Calbiochem) as described before [*34*].

Affinity purification was carried out in batch by incubation for 2 hours at 4° C with anti-FLAG resin at a 1:100 ratio. The samples were then transferred to a micro-spin column and washed with ~100 volumes (relative to the resin volume) of wash buffer (50 mM HEPES pH 7.5, 200 mM KOAc, 15 mM $MgOAc_2$, 1 mM DTT, 0.25% digitonin). Samples were eluted by incubation for 30 min at 22° C with 1 resin volume of wash buffer supplemented with 0.2 mg/mL 3X FLAG peptide, separated from the resin by a brief spin of the micro-column, and used immediately for grid preparation. The concentration of ribosomes in this final preparation was ~100 nM as judged by A_{260}. No ribosomes were recovered from reactions lacking a tagged nascent chain, verifying specificity of affinity purification.

Grid preparation and data collection

The eluted samples were applied directly to glow-discharged holey carbon grids (Quantifoil R2/2), which had been coated with a ~70 Å thick layer of amorphous carbon. Using an FEI Vitrobot, 3 μL of sample was applied to the grid, followed by a 30 sec incubation at 4° C, 9 sec of blotting, and flash-cooling in liquid ethane. Data were collected on an FEI Titan Krios at 300 KV using FEI's automated single particle acquisition software and defocus values of 2-3.5 μm. Images were recorded using a back-thinned FEI Falcon II detector at a calibrated magnification of 104,478 (pixel size of 1.34 Å). Individual frames from the detector were recorded as previously described [*35*].

Image processing

Contrast transfer function parameters were estimated using CTFFIND3 [*36*], and micrographs that had evidence of astigmatism or drift were discarded. All automated

particle picking, 2D and 3D classifications, and refinements were performed using RELION as described below [*37*]. Unsupervised 2D class averaging was used to discard any non-ribosome particles, resulting 136,639 ribosome-Sec61 particles. 3D classification was utilized to identify the population of 101,339 ribosome-Sec61 particles containing an unratcheted P-site tRNA as a proxy for presence of the nascent chain. Final 3D refinements of the resulting populations were performed utilizing statistical movie processing [*35*], and particle polishing [*38*]. This resulted in a final reconstruction at overall resolution of 3.6 Å using the gold-standard FSC=0.143 criteria [*39*].

Model building and refinement

The model for the open Sec61 channel was built using the archaeal SecY crystal structure [*2*] and the model for the idle channel [*9*]. The four transmembrane helices (6 through 9) of Sec61α that directly contact the ribosome via their associated cytosolic loops required little to no adjustments, while the remaining 6 helices (1-5, 10) and Sec61β could be rotated as a unit and fit as a rigid body with minimal adjustments into the observed density. The C-terminus of Sec61γ required further minor adjustments. After fitting of the Sec61 channel subunits, the remaining additional helical density was fit to the signal helix using a combination of the observed density, the biophysical properties of the surrounding helices, and the favourable localization of polar residues away from the lipid bilayer (fig. S8). Refinement was carried out using REFMAC v5.8 [*40*] as previously described [*41, 42*]. Secondary structure restraints were generated in ProSMART [*43*] and were maintained throughout refinement to prevent over-fitting. Local resolution was calculated using ResMap [*44*] and all figures were generated using Pymol [*45*] and Chimera [*46*].

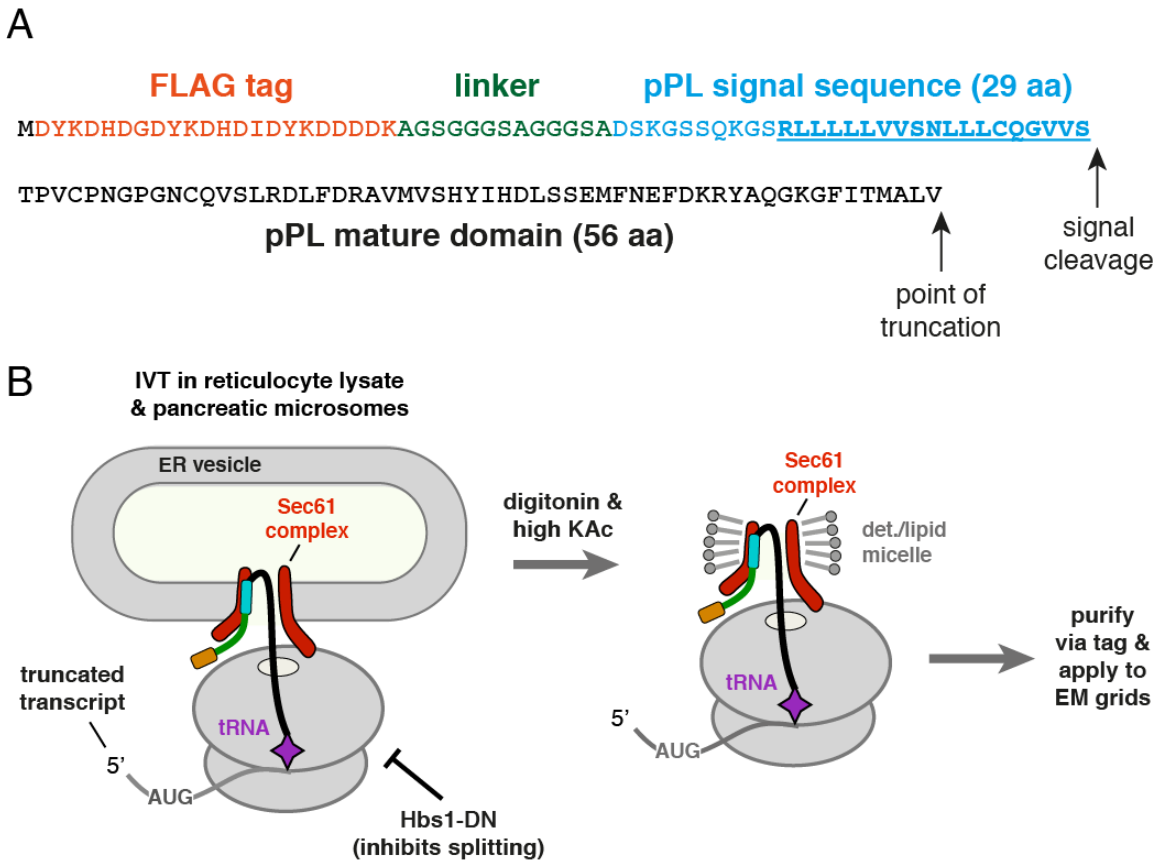

Fig. S1. Experimental strategy for sample preparation. (**A**) Sequence of the nascent chain used to engage the Sec61 complex. The 3X FLAG tag (orange) and a flexible linker (green) were inserted after the initiating methionine of pre-prolactin (pPL). The signal peptide is in cyan, and the mature domain up to residue 85 of pPL, plus a final valine, is in black. The underlined sequence was modelled in the structure. Extending the pPL signal peptide at the N-terminus is unlikely to affect its function (as verified in Figs. S2 to S4) given that the n-regions of signal peptides are highly diverse and variable in length. (**B**) Schematic of the translationally stalled substrate bound to the Sec61 complex. As shown in Fig. S2B, this complex is a functional on-pathway intermediate since release with puromycin permits translocation. Note that the GTPase-deficient Hbs1 protein included in the translation reaction prevents ribosome splitting by the ribosome-quality control pathway that ordinarily recognizes stalled ribosomes. Of the 56 residues following the signal peptide, ~35-40 residues are expected to be in the ribosomal tunnel, leaving ~16-21 residues to traverse the Sec61 channel. After assembly, the complex is solubilized using digitonin and high salt, and affinity purified via the FLAG tag before application to EM grids. As shown in Fig. S4, affinity purification does not dislodge the nascent chain from being fully inserted into the Sec61 complex.

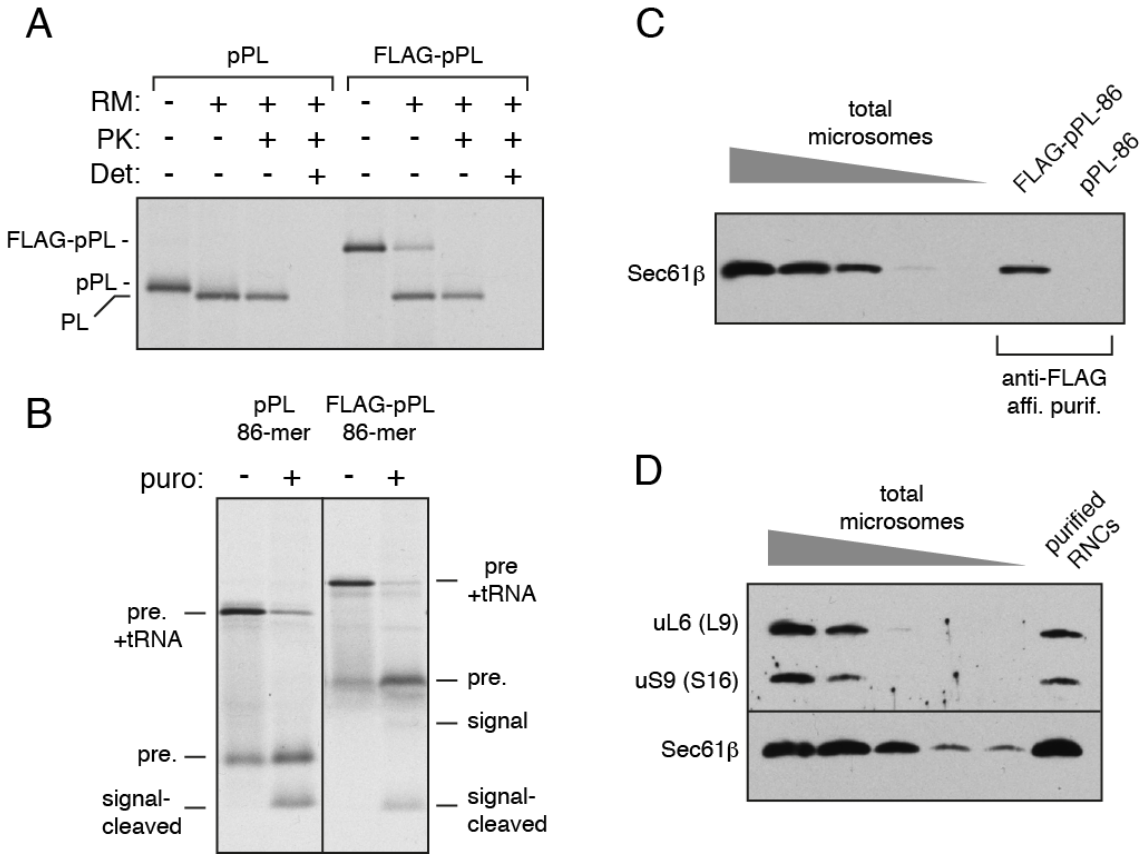

Fig. S2. Biochemical characterization of the FLAG-pPL construct. (**A**) In vitro translation reactions containing ^{35}S-methionine were programmed with transcripts coding for full length pre-prolactin (pPL) or FLAG-pPL (see Fig. S1). Reactions were performed without or with canine pancreatic rough microsomes (RM) as indicated. After translation, aliquots were digested with proteinase K (PK) in the absence or presence of the detergent (det) Triton X-100 at 0.5%. All samples were analyzed by SDS-PAGE and autoradiography. Note that both pPL and FLAG-pPL are efficiently translocated into microsomes as judged by signal peptide cleavage and protease protection of the processed product. (**B**) FLAG-pPL or untagged pPL, truncated at residue 86 (numbering of pPL), was translated in the presence of RM and ^{35}S-methionine and either left untreated or reacted with puromycin (puro) before analysis by SDS-PAGE and autoradiography. The positions of the tRNA attached precursor (pre.+tRNA), free precursor (pre.), and signal-cleaved product are indicated. Note that a small amount of tRNA is hydrolyzed during electrophoresis, but most remains attached. Treatment with puromycin hydrolyzes the tRNA, resulting in translocation of the polypeptide as judged by signal peptide cleavage. The cleaved FLAG-tagged signal is weakly visible due to it single radiolabeled methionine. (**C**) Microsomes containing the 86-mer translocation intermediate of FLAG-pPL or untagged pPL were isolated by centrifugation, solubilized with digitonin-containing buffer, and subjected to affinity purification via the FLAG tag. The eluted products were analyzed for recovery of Sec61 complex by immunoblotting relative to serial dilutions of starting microsomes. Sec61 complex is recovered only with the tagged substrate, indicating specificity of its recovery. (**D**) Immunoblotting of affinity

purified FLAG-pPL 86-mer complexes (as in panel C) for Sec61 and ribosomal proteins show that they are recovered at a ratio comparable to that observed in the starting rough microsomes.

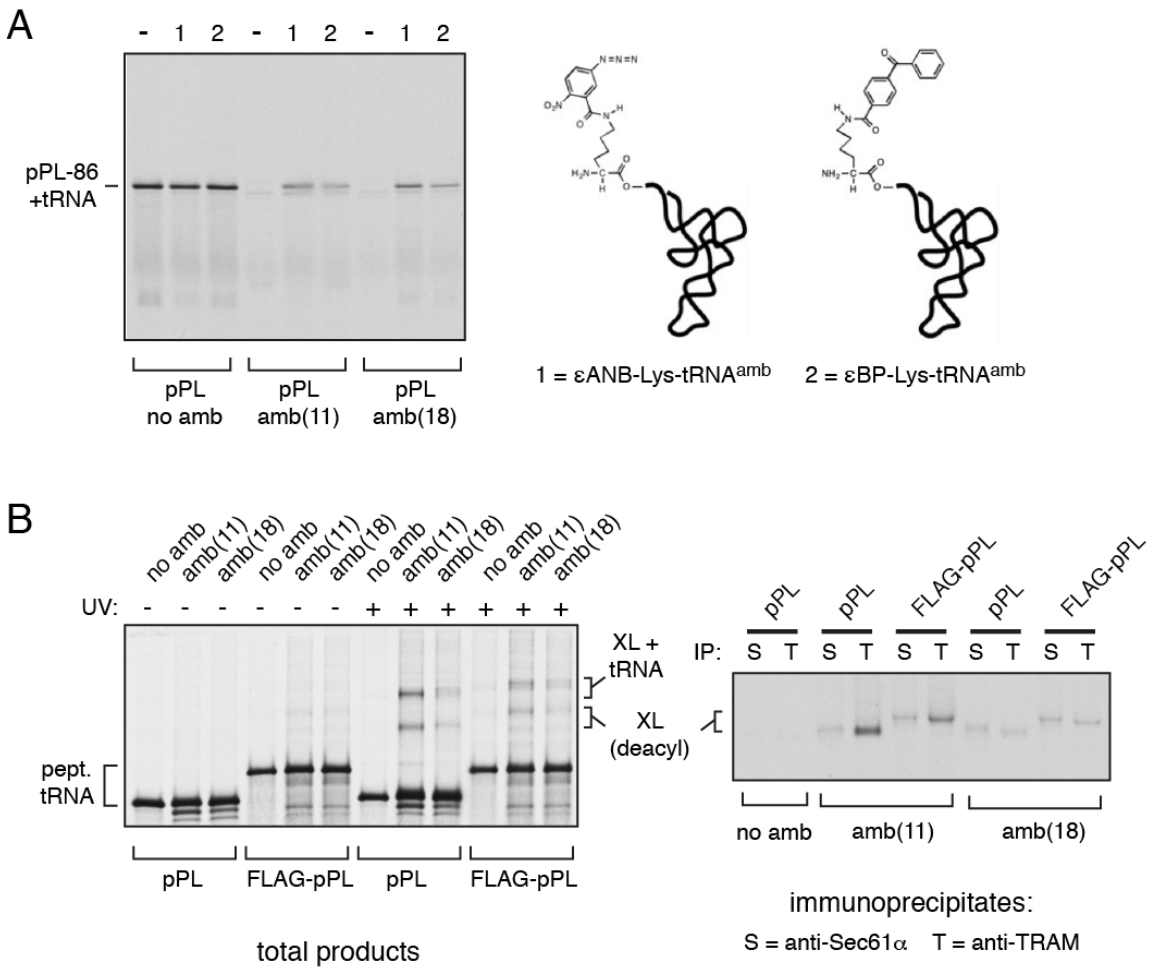

Fig. S3. Analysis of signal peptide interactions by site-specific cross-linking. (**A**) Amber codons at positions 11 or 18 were introduced into the pPL signal peptide. The 86-mer intermediate of the unmutated or amber-containing constructs was translated in vitro with ^{35}S-methionine and one of two charged amber-suppressor tRNAs whose structures are shown. Note that full length translation product (represented by the 86-mer peptidyl-tRNA) is not produced when amber codons are present unless also suppressed by either of the two tRNAs. Suppression efficiencies are ~10-25%. This permits incorporation of the indicated unnatural amino acids, both suitable for photo-cross-linking, at defined positions. (**B**) The indicated 86-mer peptidyl-tRNA intermediates of pPL or FLAG-pPL constructs were assembled on rough microsomes as in Fig. S2B. The constructs contained amber codons at the indicated positions, and the translation reactions contained the εANB-Lys-tRNA^{amb} suppressor tRNA for incorporation of photo-cross-linker. The microsomes were isolated by centrifugation, divided in two, and one half subjected to UV irradiation for 15 min to induce photo-cross-linking. An aliquot of the total products was analyzed (left panel), while the remainder was subjected to denaturing immunoprecipitation (IP) using antibodies against either Sec61α or TRAM (right panel). The left panel shows the position of the uncross-linked peptidyl-tRNA products, and the major cross-linked species. Partial deacylation of the tRNA occurs during electrophoresis, resulting in two major cross-linked bands. The IPs show that the cross-

linked band (which becomes fully deacylated during the IP) is a mixture of Sec61α and TRAM. The overall cross-linking efficiency and the ratio of Sec61 to TRAM cross-links vary depending on cross-linker position [*10-13*]. The pattern of both efficiency and ratio is the same for pPL and FLAG-pPL, strongly arguing that the two signals are positioned in the translocon in very similar ways. Similar concordance was also seen for the other cross-linker (not shown).

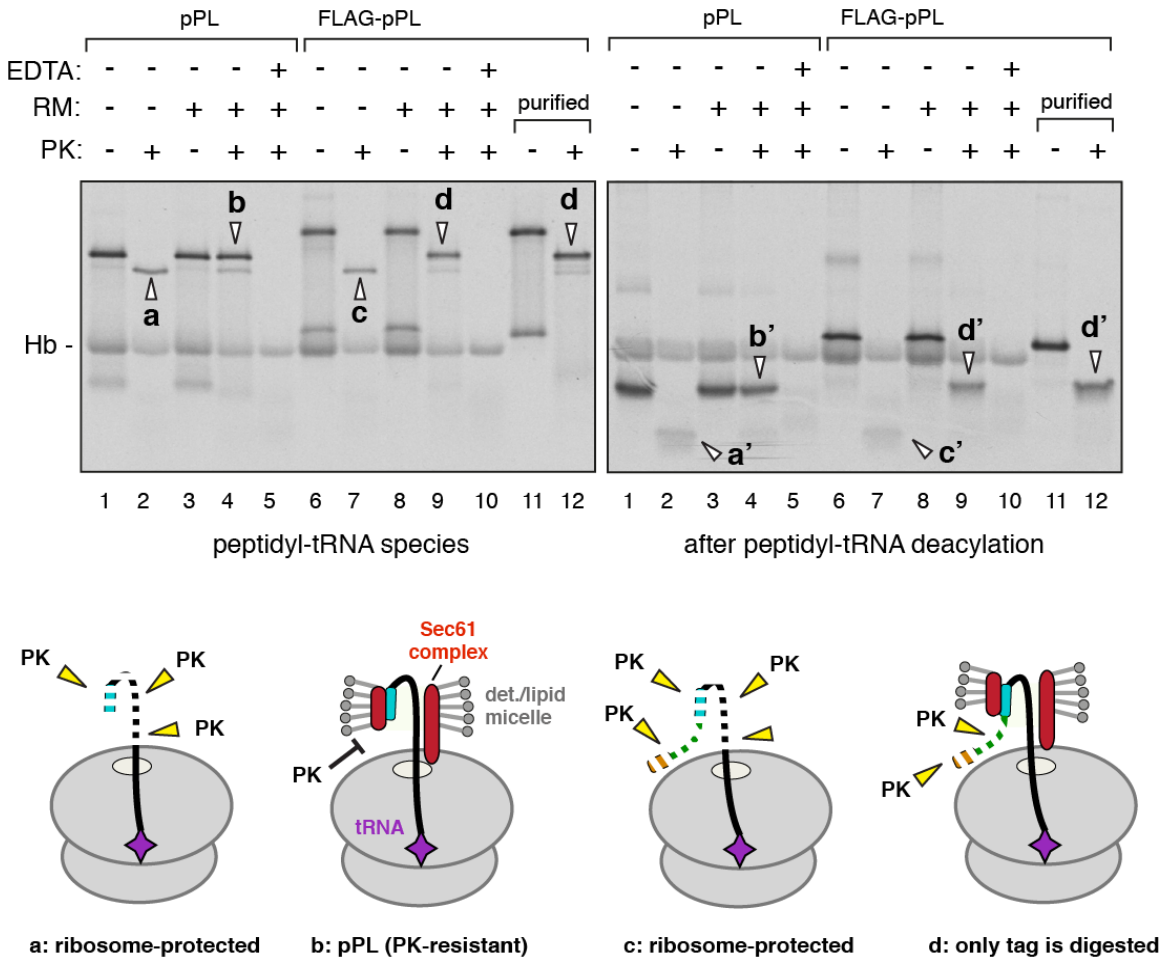

Fig. S4. Analysis of nascent chain engagement of Sec61 by protease protection. 86-mer peptidyl-tRNA translocation intermediates of either pPL or FLAG-pPL were translated with ^{35}S-methionine as in Fig. S2B in reactions that either lacked or contained rough microsomes (RM). One aliquot of the RM-targeted FLAG-pPL sample was solubilized and affinity purified using conditions identical to those for structure determination (lanes 11, 12), while the remaining samples were analyzed directly after adjusting them with 1% digitonin to dissolve the membrane. Aliquots were treated with proteinase K (PK) in the absence or presence of EDTA to disrupt the ribosome where indicated. The samples were analyzed directly to visualize the peptidyl-tRNA species (left gel) or after high pH induced hydrolysis of the tRNA (right gel). Key molecular species (a-d) are indicated with arrowheads, and the interpretations of these respective products are shown in the four diagrams under the gel. Species a' to d' are the deacylated versions of species a to d, respectively. Hb indicates haemoglobin, produced and/or labeled at low levels in the reticulocyte-based translation extract. As expected, PK digestion of pPL or FLAG-pPL in the absence of RM produces a short tRNA-attached fragment with ~35-40 residues protected by the ribosomal tunnel (lanes 2 and 7; species a and c). In the presence of RM, pPL is now fully protected due to its insertion into the Sec61 translocon (lane 4, species b) as shown previously [*12*]. By contrast, FLAG-pPL is partially protected, resulting in a tRNA-attached fragment whose size is identical to the fully protected pPL 86-mer (lane 9, species d). Thus, the FLAG tag and linker extension

are accessible to protease, while the native pPL portion of the nascent chain is shielded similarly to untagged pPL (compare diagrams b and d). This identical pattern of PK accessibility is retained on samples after they have undergone affinity purification (lane 12, compare to lane 9), strongly suggesting that nascent chain insertion into the Sec61 translocon is not disrupted by the purification process.

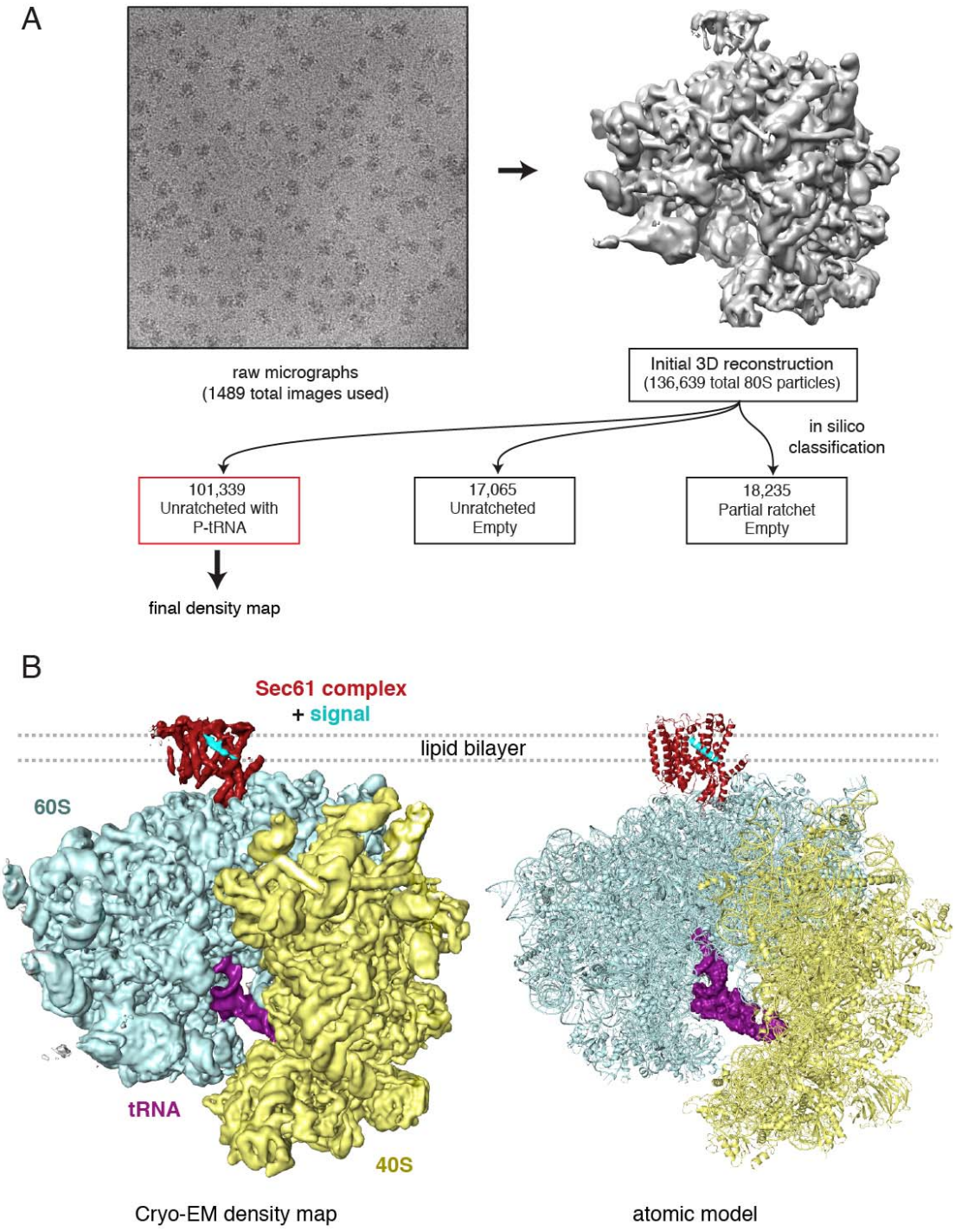

Fig. S5. Overview of particle classification and structure determination. (**A**) Schematic of the data collection and particle classification scheme used to derive the final density map. Note that the initial 3D reconstruction of all particles from down-sampled micrographs without movie processing or particle polishing already shows very clear density for the Sec61 complex in which individual transmembrane helices are readily visible, including the signal peptide. At this threshold, the detergent micelle surrounding

the Sec61 complex is not visible due to its heterogeneity relative to the homogeneous and defined positions of the transmembrane helices of the Sec61 complex (and of course, the ribosome). From this total particle dataset, in silico classification was used to identify the ~74% of particles containing an unratcheted ribosome and P-site tRNA, which was used as a surrogate to identify those particles containing a nascent chain. This subset was used to produce the final density map. (**B**) The unsharpened EM density map (left panel) is shown with the final molecular model (right panel). The components are colored as follows: 40S subunit (yellow), 60S subunit (blue), the peptidyl-tRNA (purple), the Sec61 channel (red), and the signal peptide (cyan). Note that this is the raw density map shown at a single threshold without any segmentation. At the displayed threshold where each of the individual transmembrane helices of the Sec61 complex and the signal peptide are clearly visible and resolved, the detergent-lipid micelle is not observed. Thus, the occupancy and homogeneity of the signal-Sec61 complex is very high, suggesting that it represents a single uniform conformation.

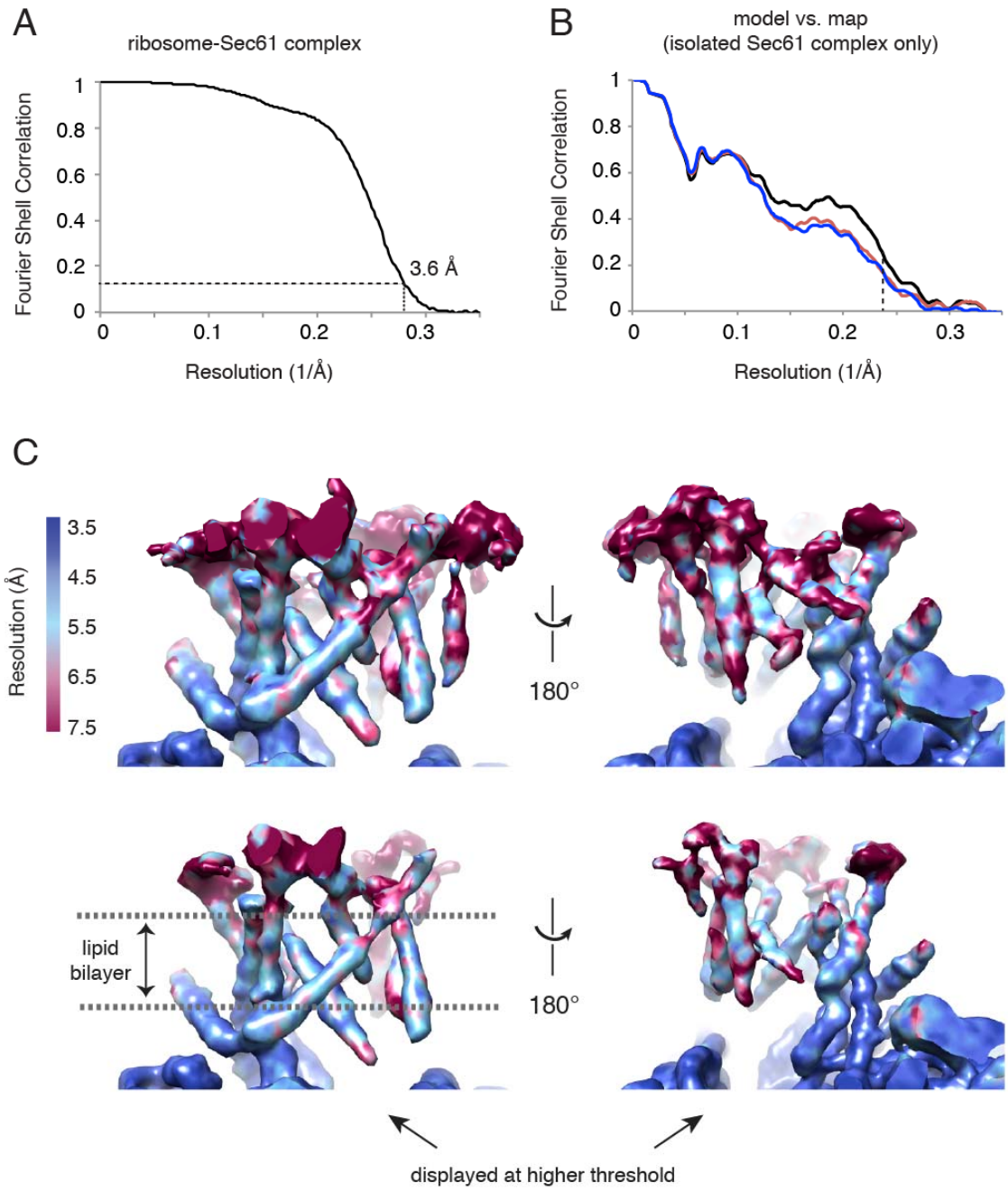

Fig. S6. Map and model quality. (**A**) Gold-standard Fourier Shell Correlation (FSC) curve for the map of the engaged ribosome-Sec61 complex where the overall resolution is demarcated using the FSC=0.143 criterion. (**B**) FSC curves for the isolated Sec61 region of the map. The curve for the final model versus the map derived from the complete dataset is shown in black; red shows the curve for a model refined in the first of two independent halves of the map; and blue shows that same model versus the second independent half-map, which was not used for refinement. The vertical dashed line indicates the highest resolution (4.25 Å) used in these model refinements. (**C**) Local resolution of the engaged channel, produced using ResMap [*44*], shown from either the Sec61γ side (left) or lateral gate (right). Two different thresholds are displayed in the

upper and lower panels. The resolution of the Sec61 regions contacting the ribosome approach ~3.5 Å resolution, while the flexible loops on the lumenal side of Sec61 are ~7 Å. In regions of Sec61 that are in the membrane (demarcated in the lower-left panel), most of the TM helices range between ~4.0-5.5 Å resolution.

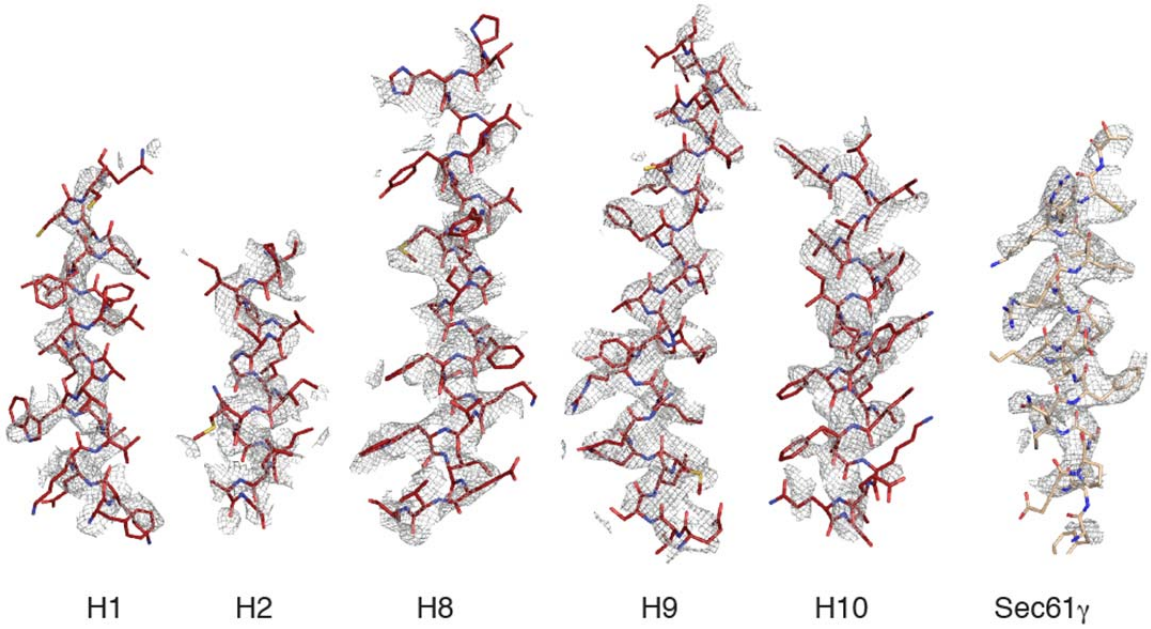

Fig. S7. Examples of map quality. Representative density from sharpened maps for several of the TM helices from the Sec61 complex, filtered to 3.8 Å, and their associated molecular models. The quality of the data is such that placement of the helix and the helical pitch is unambiguous for all helices in the channel, while many amino acid side chains are visible in both the stationary (helices 6-9, γ) and mobile (1-5,10, β) portions of Sec61.

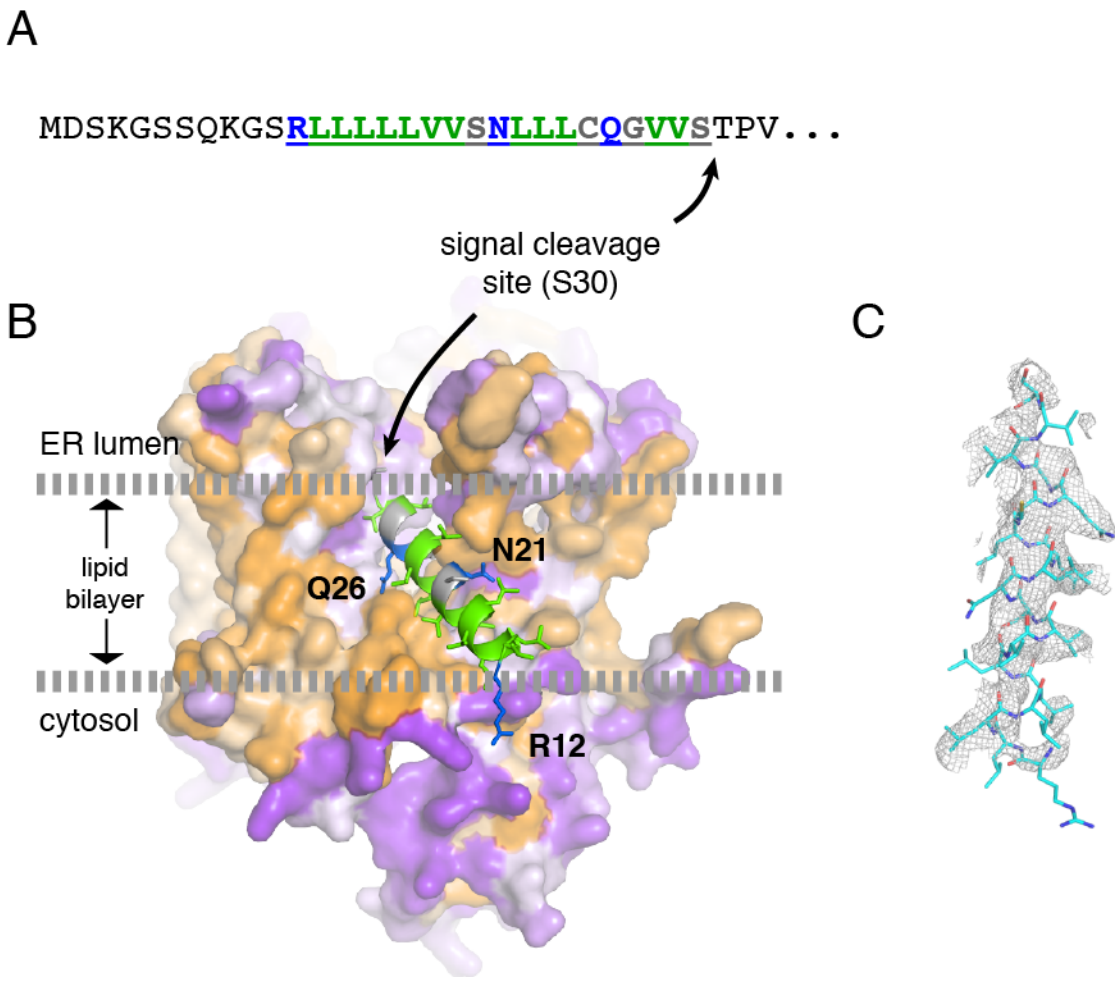

Fig. S8. Assignment of a likely registry for the signal peptide relative to Sec61. The sequence of the pPL signal peptide is shown, with the region modelled in our map underlined. Highly hydrophilic/polar residues are indicated in blue, while highly hydrophobic residues are green. The position of signal cleavage is indicated. (**A**) Signal sequence. (**B**) Shown is a space filling model of the engaged Sec61 complex colored by hydrophobicity, with orange indicating hydrophobic and purple hydrophilic surfaces. The signal sequence helix is shown with sticks for side chains, colored using the same scheme as in (A). The three particularly hydrophilic residues are unlikely to be facing lipid or the hydrophobic surface of Sec61. Hence, a registry was chosen that not only best matches with the density map (C), but also one in which hydrophilic residues can either snorkel to the lipid head groups (R12) or face hydrophilic regions on Sec61 (N21 and Q26). Conversely, the hydrophobic residues primarily face either lipid or hydrophobic Sec61 surfaces. Finally, the signal peptide cleavage site is likely to be at the lumenal side of the lipid bilayer, since it will eventually be accessed by signal peptidase whose active site is in the lumen. Conversely, the sequences preceding R12 (not modelled) are likely to be facing the cytosol and outside the lipid bilayer given their high hydrophilicity. Thus, the chosen registry fits best with known biological activities (site of signal cleavage and n-region facing the cytosol) as well as biophysical considerations. Other registries for the signal peptide either did not fit as well into the density map or resulted in unfavorable

hydrophobic mismatch. (**C**) The density map for the modelled region of the signal peptide (grey mesh) shown with the final atomic model (cyan) as in Fig. S7.

Table S1. Refinement and model statistics.

Data collection	
Particles	101,339
Pixel size (Å)	1.34
Defocus range (mm)	2.0-3.5
Voltage (kV)	300
Electron dose (e/Å^2)	27
Map sharpening B-factor (Å^2)	-72.6
Model composition	**Engaged Sec61**
Non-hydrogen atoms	3,912
Protein residues	514
Refinement	
Resolution used (Å)	4.25
Average B factor (Å^2)	156
Fourier shell correlation (FSC)*	0.72
Rms deviations	
Bonds (Å)	0.011
Angles (°)	1.5
Ramachandran plot	
Favored (%)	94
Outliers (%)	6

*FSC = $\Sigma(F_{obs}\, F^*_{calc}) / \sqrt{(\Sigma|F_{obs}|^2\, \Sigma|F_{calc}|^2)}$

Table S2. Conserved residues of key functional motifs.

Motif	***H. sapiens* residues**	***M. jannaschii* residues**
Polar Cluster	T86	T80
	Q127	E122
	N300	N268
Pore ring	I81	I75
	V85	V79
	I179	I170
	I183	I174
	I292	I260
	L449	L406
Hydrophobic patch	V85	V79
	L89	I83
	I179	I170
	I293	L261

Movie S1. Morph between the ribosome-primed idle Sec61 complex (3J7Q) and the engaged Sec61 complex. The view is from the plan of the membrane looking toward the lateral gate; the ribosome would be on the bottom and ER lumen on the top. Only the transmembrane segments and the ribosome-interacting cytosolic loops are shown for clarity. Sec61 α, β, and γ are in red, light blue, and tan, respectively. The signal sequence (cyan) appears in the engaged state at its position in the lateral gate.

Movie S2. Morph between the ribosome-primed idle Sec61 complex (3J7Q) and the engaged Sec61 complex as viewed from the ER lumen. The lateral gate is on the bottom. Only the transmembrane segments are depicted for clarity. At the beginning of the animation, Sec61α, β, and γ are in red, light blue, and tan, respectively. The helices that rotate as a rigid body turn grey just before their movement. The signal sequence (cyan) appears in the engaged state at the end of the animation.

REFERENCES AND NOTES

1. E. Park, T. A. Rapoport, Mechanisms of Sec61/SecY-mediated protein translocation across membranes. *Annu. Rev. Biophys.* **41**, 21–40 (2012). Medline doi:10.1146/annurev-biophys-050511-102312

2. B. Van den Berg, W. M. Clemons Jr., I. Collinson, Y. Modis, E. Hartmann, S. C. Harrison, T. A. Rapoport, X-ray structure of a protein-conducting channel. *Nature* **427**, 36–44 (2004). Medline doi:10.1038/nature02218

3. K. Plath, W. Mothes, B. M. Wilkinson, C. J. Stirling, T. A. Rapoport, Signal sequence recognition in posttranslational protein transport across the yeast ER membrane. *Cell* **94**, 795–807 (1998). Medline doi:10.1016/S0092-8674(00)81738-9

4. P. F. Egea, R. M. Stroud, Lateral opening of a translocon upon entry of protein suggests the mechanism of insertion into membranes. *Proc. Natl. Acad. Sci. U.S.A.* **107**, 17182–17187 (2010). Medline doi:10.1073/pnas.1012556107

5. T. Tsukazaki, H. Mori, S. Fukai, R. Ishitani, T. Mori, N. Dohmae, A. Perederina, Y. Sugita, D. G. Vassylyev, K. Ito, O. Nureki, Conformational transition of Sec machinery inferred from bacterial SecYE structures. *Nature* **455**, 988–991 (2008). Medline doi:10.1038/nature07421

6. J. Zimmer, Y. Nam, T. A. Rapoport, Structure of a complex of the ATPase SecA and the protein-translocation channel. *Nature* **455**, 936–943 (2008). Medline doi:10.1038/nature07335

7. M. Gogala, T. Becker, B. Beatrix, J. P. Armache, C. Barrio-Garcia, O. Berninghausen, R. Beckmann, Structures of the Sec61 complex engaged in nascent peptide translocation or membrane insertion. *Nature* **506**, 107–110 (2014). Medline doi:10.1038/nature12950

8. E. Park, J. F. Ménétret, J. C. Gumbart, S. J. Ludtke, W. Li, A. Whynot, T. A. Rapoport, C. W. Akey, Structure of the SecY channel during initiation of protein translocation. *Nature* **506**, 102–106 (2014). Medline doi:10.1038/nature12720

9. R. M. Voorhees, I. S. Fernández, S. H. W. Scheres, R. S. Hegde, Structure of the mammalian ribosome-Sec61 complex to 3.4 Å resolution. *Cell* **157**, 1632–1643 (2014). Medline doi:10.1016/j.cell.2014.05.024

10. S. High *et al*., Site-specific photocross-linking reveals that Sec61p and TRAM contact different regions of a membrane-inserted signal sequence. *J. Biol. Chem.* **268**, 26745–26751 (1993). Medline

11. W. Mothes, S. Prehn, T. A. Rapoport, Systematic probing of the environment of a translocating secretory protein during translocation through the ER membrane. *EMBO J.* **13**, 3973–3982 (1994). Medline

12. B. Jungnickel, T. A. Rapoport, A posttargeting signal sequence recognition event in the endoplasmic reticulum membrane. *Cell* **82**, 261–270 (1995). Medline doi:10.1016/0092-8674(95)90313-5

13. W. Mothes, B. Jungnickel, J. Brunner, T. A. Rapoport, Signal sequence recognition in cotranslational translocation by protein components of the endoplasmic reticulum

membrane. *J. Cell Biol.* **142**, 355–364 (1998). Medline doi:10.1083/jcb.142.2.355

14. K. S. Crowley, S. Liao, V. E. Worrell, G. D. Reinhart, A. E. Johnson, Secretory proteins move through the endoplasmic reticulum membrane via an aqueous, gated pore. *Cell* **78**, 461–471 (1994). Medline doi:10.1016/0092-8674(94)90424-3

15. B. Martoglio, M. W. Hofmann, J. Brunner, B. Dobberstein, The protein-conducting channel in the membrane of the endoplasmic reticulum is open laterally toward the lipid bilayer. *Cell* **81**, 207–214 (1995). Medline doi:10.1016/0092-8674(95)90330-5

16. S. Pfeffer, L. Burbaum, P. Unverdorben, M. Pech, Y. Chen, R. Zimmermann, R. Beckmann, F. Förster, Structure of the native Sec61 protein-conducting channel. *Nat. Commun.* **6**, 8403 (2015). 10.1038/ncomms9403 Medline doi:10.1038/ncomms9403

17. Although P-site transfer RNA was absent from the majority of ribosomes used for the cryo-tomography structure (*16*), the presence or absence of heterogeneous endogenous nascent polypeptides within Sec61 could not be determined conclusively. Thus, the conclusion that the Sec61 complex is constitutively open upon ribosome binding, independent of substrate or functional state, may be premature. Indeed, biochemical studies in native microsomes show substrate-induced Sec61 opening (*14*), no translocation of Sec61-docked polypeptides with a mutant signal (*12*), and no lipid access to early translocation intermediates (*13*). Genetic studies show that modulation of lateral gate interactions influences translocation (*20–27*). Thus, multiple independent findings argue that substrates induce structural changes to the Sec61 complex that open it laterally.

18. R. M. Voorhees, R. S. Hegde, Structures of the scanning and engaged states of the mammalian SRP-ribosome complex. *eLife* **4**, e07975 (2015). Medline doi:10.7554/eLife.07975

19. K. S. Crowley, G. D. Reinhart, A. E. Johnson, The signal sequence moves through a ribosomal tunnel into a noncytoplasmic aqueous environment at the ER membrane early in translocation. *Cell* **73**, 1101–1115 (1993). Medline doi:10.1016/0092-8674(93)90640-C

20. T. Junne, T. Schwede, V. Goder, M. Spiess, Mutations in the Sec61p channel affecting signal sequence recognition and membrane protein topology. *J. Biol. Chem.* **282**, 33201–33209 (2007). Medline doi:10.1074/jbc.M707219200

21. M. A. Smith, W. M. J. Clemons Jr., C. J. DeMars, A. M. Flower, Modeling the effects of *prl* mutations on the *Escherichia coli* SecY complex. *J. Bacteriol.* **187**, 6454–6465 (2005). Medline doi:10.1128/JB.187.18.6454-6465.2005

22. A. I. Derman, J. W. Puziss, P. J. J. Bassford Jr., J. Beckwith, A signal sequence is not required for protein export in *prlA* mutants of *Escherichia coli*. *EMBO J.* **12**, 879–888 (1993). Medline

23. R. S. Osborne, T. J. Silhavy, *PrlA* suppressor mutations cluster in regions corresponding to three distinct topological domains. *EMBO J.* **12**, 3391–3398

(1993). Medline

24. A. P. Maillard, S. Lalani, F. Silva, D. Belin, F. Duong, Deregulation of the SecYEG translocation channel upon removal of the plug domain. *J. Biol. Chem.* **282**, 1281–1287 (2007). Medline doi:10.1074/jbc.M610060200

25. S. F. Trueman, E. C. Mandon, R. Gilmore, A gating motif in the translocation channel sets the hydrophobicity threshold for signal sequence function. *J. Cell Biol.* **199**, 907–918 (2012). Medline doi:10.1083/jcb.201207163

26. A. L. Mackinnon, V. O. Paavilainen, A. Sharma, R. S. Hegde, J. Taunton, An allosteric Sec61 inhibitor traps nascent transmembrane helices at the lateral gate. *eLife* **3**, e01483 (2014). Medline doi:10.7554/eLife.01483

27. T. Junne, J. Wong, C. Studer, T. Aust, B. W. Bauer, M. Beibel, B. Bhullar, R. Bruccoleri, J. Eichenberger, D. Estoppey, N. Hartmann, B. Knapp, P. Krastel, N. Melin, E. J. Oakeley, L. Oberer, R. Riedl, G. Roma, S. Schuierer, F. Petersen, J. A. Tallarico, T. A. Rapoport, M. Spiess, D. Hoepfner, Decatransin, a new natural product inhibiting protein translocation at the Sec61/SecYEG translocon. *J. Cell Sci.* **128**, 1217–1229 (2015). Medline doi:10.1242/jcs.165746

28. S. Shao, K. von der Malsburg, R. S. Hegde, Listerin-dependent nascent protein ubiquitination relies on ribosome subunit dissociation. *Mol. Cell* **50**, 637–648 (2013). Medline doi:10.1016/j.molcel.2013.04.015

29. S. Shao, R. S. Hegde, Reconstitution of a minimal ribosome-associated ubiquitination pathway with purified factors. *Mol. Cell* **55**, 880–890 (2014). Medline doi:10.1016/j.molcel.2014.07.006

30. R. D. Fons, B. A. Bogert, R. S. Hegde, Substrate-specific function of the translocon-associated protein complex during translocation across the ER membrane. *J. Cell Biol.* **160**, 529–539 (2003). Medline doi:10.1083/jcb.200210095

31. A. Sharma, M. Mariappan, S. Appathurai, R. S. Hegde, In vitro dissection of protein translocation into the mammalian endoplasmic reticulum. *Methods Mol. Biol.* **619**, 339–363 (2010). Medline doi:10.1007/978-1-60327-412-8_20

32. P. Walter, G. Blobel, Preparation of microsomal membranes for cotranslational protein translocation. *Methods Enzymol.* **96**, 84–93 (1983). Medline doi:10.1016/S0076-6879(83)96010-X

33. S. J. Kim, R. S. Hegde, Cotranslational partitioning of nascent prion protein into multiple populations at the translocation channel. *Mol. Biol. Cell* **13**, 3775–3786 (2002). Medline doi:10.1091/mbc.E02-05-0293

34. D. Görlich, T. A. Rapoport, Protein translocation into proteoliposomes reconstituted from purified components of the endoplasmic reticulum membrane. *Cell* **75**, 615–630 (1993). Medline doi:10.1016/0092-8674(93)90483-7

35. X.-C. Bai, I. S. Fernandez, G. McMullan, S. H. W. Scheres, Ribosome structures to near-atomic resolution from thirty thousand cryo-EM particles. *eLife* **2**, e00461 (2013). Medline doi:10.7554/eLife.00461

36. J. A. Mindell, N. Grigorieff, Accurate determination of local defocus and specimen

tilt in electron microscopy. *J. Struct. Biol.* **142**, 334–347 (2003). Medline doi:10.1016/S1047-8477(03)00069-8

37. S. H. W. Scheres, RELION: Implementation of a Bayesian approach to cryo-EM structure determination. *J. Struct. Biol.* **180**, 519–530 (2012). Medline doi:10.1016/j.jsb.2012.09.006

38. S. H. Scheres, Beam-induced motion correction for sub-megadalton cryo-EM particles. *eLife* **3**, e03665 (2014). Medline doi:10.7554/eLife.03665

39. S. H. W. Scheres, S. Chen, Prevention of overfitting in cryo-EM structure determination. *Nat. Methods* **9**, 853–854 (2012). Medline doi:10.1038/nmeth.2115

40. G. N. Murshudov, P. Skubák, A. A. Lebedev, N. S. Pannu, R. A. Steiner, R. A. Nicholls, M. D. Winn, F. Long, A. A. Vagin, REFMAC5 for the refinement of macromolecular crystal structures. *Acta Crystallogr. D Biol. Crystallogr.* **67**, 355–367 (2011). Medline doi:10.1107/S0907444911001314

41. A. Amunts, A. Brown, X. C. Bai, J. L. Llácer, T. Hussain, P. Emsley, F. Long, G. Murshudov, S. H. Scheres, V. Ramakrishnan, Structure of the yeast mitochondrial large ribosomal subunit. *Science* **343**, 1485–1489 (2014). Medline doi:10.1126/science.1249410

42. A. Brown, F. Long, R. A. Nicholls, J. Toots, P. Emsley, G. Murshudov, Tools for macromolecular model building and refinement into electron cryo-microscopy reconstructions. *Acta Crystallogr. D Biol. Crystallogr.* **71**, 136–153 (2015). Medline doi:10.1107/S1399004714021683

43. R. A. Nicholls, F. Long, G. N. Murshudov, Low-resolution refinement tools in REFMAC5. *Acta Crystallogr. D Biol. Crystallogr.* **68**, 404–417 (2012). Medline doi:10.1107/S090744491105606X

44. A. Kucukelbir, F. J. Sigworth, H. D. Tagare, Quantifying the local resolution of cryo-EM density maps. *Nat. Methods* **11**, 63–65 (2014). Medline doi:10.1038/nmeth.2727

45. W. L. DeLano, *The PyMOL Molecular Graphics System* (DeLano Scientific, Palo Alto, CA, 2006); www.pymol.org.

46. T. D. Goddard, C. C. Huang, T. E. Ferrin, Visualizing density maps with UCSF Chimera. *J. Struct. Biol.* **157**, 281–287 (2007). Medline doi:10.1016/j.jsb.2006.06.010